Am J Physiol Heart Circ Physiol
280: H2689–H2696, 2001.

Effects of diacetyl monoxime and cytochalasin D on ventricular fibrillation in swine right ventricles

MOON-HYOUNG LEE,[1] SHIEN-FONG LIN,[2] TOSHIHIKO OHARA,[1] CHIKAYA OMICHI,[1] YUJI OKUYAMA, EUGENE CHUDIN,[3] ALAN GARFINKEL,[3] JAMES N. WEISS,[3] HRAYR S. KARAGUEUZIAN,[1] AND PENG-SHENG CHEN[1]

[1]*Division of Cardiology, Department of Medicine, Cedars-Sinai Medical Center, and* [2]*Division of Cardiology, Departments of Medicine and Physiology and Physiological Science, University of California School of Medicine, Los Angeles, California 90048; and* [3]*Department of Physics and Astronomy, Vanderbilt University, Nashville, Tennessee 37235*

Received 13 June 2000; accepted in final form 29 January 2001

Lee, Moon-Hyoung, Shien-Fong Lin, Toshihiko Ohara, Chikaya Omichi, Yuji Okuyama, Eugene Chudin, Alan Garfinkel, James N. Weiss, Hrayr S. Karagueuzian, and Peng-Sheng Chen. Effects of diacetyl monoxime and cytochalasin D on ventricular fibrillation in swine right ventricles. *Am J Physiol Heart Circ Physiol* 280: H2689–H2696, 2001.—Whether or not the excitation-contraction (E-C) uncoupler diacetyl monoxime (DAM) and cytochalacin D (Cyto D) alter the ventricular fibrillation (VF) activation patterns is unclear. We recorded single cell action potentials and performed optical mapping in isolated perfused swine right ventricles (RV) at different concentrations of DAM and Cyto D. Increasing the concentration of DAM results in progressively shortened action potential duration (APD) measured to 90% repolarization, reduced the slope of the APD restitition curve, decreased Kolmogorov-Sinai entropy, and reduced the number of VF wave fronts. In all RVs, 15–20 mmol/l DAM converted VF to ventricular tachycardia (VT). The VF could be reinduced after the DAM was washed out. In comparison, Cyto D (10–40 μmol/l) has no effects on APD restitution curve or the dynamics of VF. The effects of DAM on VF are associated with a reduced number of wave fronts and dynamic complexities in VF. These results are compatible with the restitution hypothesis of VF and suggest that DAM may be unsuitable as an E-C uncoupler for optical mapping studies of VF in the swine RVs.

action potentials; defibrillation; electrophysiology; reentry; tachyarrhythmias

OPTICAL MAPPING TECHNIQUES are now commonly used in the study of ventricular fibrillation (VF) and defibrillation. A benefit of these techniques is that they provide information on both the depolarization and the repolarization of cardiac action potentials. This information is crucial to the understanding of reentrant wave fronts (spiral waves), wave breaks, and VF. However, a major technical difficulty in applying optical mapping techniques to the study of cardiac activation is the vigorous contraction of the myocardium that distorts the optical signals by the introduction of motion artifacts. One way to overcome this technical difficulty is to use an excitation-contraction (E-C) uncoupler, such as diacetyl monoxime (DAM, or 2,3-butanedione monoxime, BDM) (1, 9, 10, 14, 20, 28), to immobilize the tissue. However, DAM also alters the membrane ionic currents and action potential properties (3, 8, 26). Recently, Riccio et al. (30) showed that DAM prevents the induction of VF and converts existing VF into a stable periodic rhythm by reducing the slope of the action potential duration (APD) restitution (APDR) curve. However, in that study, no mapping was performed, leaving the effects of DAM on patterns of activation undefined. The purpose of the present study was to perform optical mapping studies in swine right ventricles (RV) to determine the effects of DAM on the patterns of activation during VF at concentrations routinely used to immobilize the tissue. We also sought to determine whether or not these changes occur in parallel with changes in the slope of ADPR curve. A third aim was to study whether or not cytochalasin D (Cyto D), an E-C uncoupler without significant effects on APD in canine heart (3, 38), alters the slope of the APDR curve or the patterns of activation during VF.

METHODS

Tissue preparation and optical mapping. The details of this swine model are similar to those reported elsewhere (19). Briefly, the chest was opened, and the heart was quickly removed. The right coronary artery was cannulated, and the RV was isolated and continuously perfused with oxygenated Tyrode solution (37 ± 0.5°C, pH 7.4 ± 0.5) for the study of DAM ($n = 6$) or Cyto D ($n = 6$). The composition of the Tyrode solution was as follows (in mM): 125.0 NaCl, 4.5 KCl, 0.5 $MgCl_2$, 0.54 $CaCl_2$, 1.2 NaH_2PO_4, 24.0 $NaHCO_3$, and 5.5 glucose and included 50 mg/l albumin. The RV was paced at 400-ms cycle lengths. The RVs were stained for 20 min with di-4-ANEPPS (20 min; 1 μmol/l) through coronary perfusion. After the dye staining was completed, VF was induced by rapid electrical stimulation, and the patterns of activation

Address for reprint requests and other correspondence: P.-S. Chen, Rm. 5342, CSMC, 8700 Beverly Blvd., Los Angeles, CA 90048 (E-mail: chenp@csmc.edu).

The costs of publication of this article were defrayed in part by the payment of page charges. The article must therefore be hereby marked "*advertisement*" in accordance with 18 U.S.C. Section 1734 solely to indicate this fact.

were mapped during VF. Simultaneous single cell transmembrane potential (TMP) recordings were performed using standard glass electrodes. The RV was then electrically defibrillated. TMP and pseudoelectrocardiograms were recorded during dynamic pacing through a pair of bipolar electrodes and during sustained VF. The dynamic pacing protocol was as follows (35). We first paced the RV at a 400-ms pacing interval using twice the diastolic threshold current for eight beats, which was then followed immediately by eight beats of pacing at 350-, 300-, 280-, 260-, 240-, 230-, 220-, 210-, 200-, 190-, 180-, 170-, and 150-ms cycle lengths (CL). TMP recordings obtained during the dynamic pacing protocol were used to construct the APDR curve. Afterward, the perfusate was changed to Tyrode solution containing increasing concentrations of DAM (5, 10, 15, and 20 mmol/l) or Cyto D (10, 20, and 40 μmol/l). The experimental protocol was then repeated after each concentration of the uncouplers and after washout.

The optical mapping system is similar to the ones described previously (24, 25). A stabilized 250-W tungsten-halogen lamp (model 66196, Oriel; Stratford, CT) filtered with a bandpass filter (510 ± 40 nm) or a 5-W solid-state laser (Verdi, Coherent, Laser Group; Santa Clara, CA) at a wavelength of 532 nm was used for a light source; the induced fluorescence was collected through a 600-nm long-pass glass filter (R60, Nikon; Tokyo, Japan) with a 12-bit digital charge-coupled device camera (CA-D1–0256T or CA-D1–0128T, Dalsa; Ontario, Canada). In the study using DAM, the tungsten-halogen light source and the large format camera (CA-D1–0256T, 2 × 2 binning) was used. The camera acquired data at 3.75-ms intervals from 96 × 96 sites simultaneously over a 35 × 35-mm^2 area, resulting in a spatial resolution of 0.36 mm per pixel. The Cyto D studies were performed after the laser light source and the faster, small-format camera (CA-D1–0128T) were installed, which allowed us to acquire data at 2-ms intervals from 128 × 128 sites simultaneously over a 35 × 35-mm^2 area, resulting in a spatial resolution of 0.27 mm per pixel. The digital images were transferred to a personal computer with a frame grabber (IC-PCI-DIG16, Imaging Technology; Bedford, MA). During the experiment, the tissue was immobilized by pinning it to the base of the tissue chamber.

Signal processing. The optical signals were temporally filtered and spatially averaged to reduce noise. For temporal filtering, we applied a five-point time median filter to each pixel. We take the original first five data points (we call them *frames 1, 2, 3, 4,* and *5*) and then find the median value of those points and use that as the new value for *point 3* (i.e., *frame 3*). We then take the next original five points (i.e., *frames 2, 3, 4, 5,* and *6*) and find the median value of those and use that as the new value for *point 4*. We continue this exercise until the end of the data. We then take the tracing, invert the data, and bring the baseline down to zero, which is defined by the average of the five lowest fluorescent values recorded by that pixel. Afterward, we range normalized each pixel. We find the five lowest and five highest points and take the average of those numbers. We then adjust each fluorescent value of the pixel by the same amount so that the highest pixel value will be 255 and the lowest will be 0. Next, for each pixel on the frame, we average the fluorescent values of the pixel and its eight surrounding pixels. We use this average as the new value for the pixel. At completion of those averaging procedures, we repeated the procedure for a second time. At that time, we rezeroed the signal by bringing the baseline down to zero, defined by the average of the five lowest points of each pixel. We then range normalized the signals again. Temporal resolution is unaffected by moving median filters. Spatial resolution was reduced by the 3 × 3 moving spatial average filter, applied twice, by a factor ×2.5 from 0.27 to 0.68 mm.

The fluorescence was converted to pseudocolor animation for analysis. The maximal signal amplitude was coded yellow, representing a fully depolarized state. The minimum signal amplitude was coded black, representing a fully repolarized state. Each depolarizing pixel was then assigned a color of 128 colors among black, red, and yellow; a repolarizing pixel was assigned a color of 128 colors among yellow, green, and black. To quantify the effects of DAM or Cyto D on the patterns of epicardial activation waves, we counted the number of wavelets in every 100th frame and then averaged the number of the wavelets. We defined the number of wavelets at a given instant of VF/VT (where VT is ventricular tachycardia) as the number of activations that were independently excited over at least two frames in different areas of the mapped tissue that had different directions of propagation and were clearly separated from each other by recovered but nonactivated tissue.

Transmembrane potential, degree of disorder, and dynamic restitution. We determined peaks of TMP, interactivation interval, APD at 90% repolarization (APD_{90}), and diastolic interval (DI) using methods published elsewhere (19). The APDR curve was created by plotting APD_{90} against the preceding DI. The restitution curve was generated by exponential fit using ORIGIN 5.0 (Microcal Software, Northampton, MA). Poincaré plots were constructed by plotting each successive interactivation interval against its previous value (12).

VF is a highly irregular and disordered rhythm. However, there might be different degrees of disorder among different episodes of VF. If there is a dose-related effect of DAM or Cyto D on VF, then the disorder should change according to the concentration of drugs used. To quantify the degree of disorder (21, 33), we calculated Kolmogorov-Sinai entropy (KE) using two different methods (19). A typical time series for analysis consisted of a 20-s record of membrane potential digitized at 5 kHz. The state-space dimension, as determined by the method of false nearest neighbors, was 5. *Method A* follows Hilborn (17) and is similar to the method we used previously (19). The second method of estimating KE, *method B,* was by direct implementation of the concept "rate of invasion of new boxes." We kept track of which boxes were invaded by the state-point trajectory for the first 90–95% of each run and then calculated the percentage of all boxes encountered in the last 5–10%, which were "new." This method proved robust to changes in the side length of the box, as well as other parameters, such as the fraction of runs considered new. The laboratory of Chen et al. (19) previously reported that entropy is a useful method in measuring disorder in the swine RV preparation.

The APDR curve, Poincaré plots, and entropy analyses were generated from action potential data as recorded by a microelectrode, rather than from the optical recordings.

Statistical analysis. All data were presented as means ± SD. Student's *t*-tests were used to compare the means. ANOVA with Newman-Keuls test was used when multiple comparisons were performed. Pearson correlation was used to compare the means of the maximum slope of APDR curve and the KE. The generation of restitution curves and all statistical analyses were performed with the use of ORIGIN (Microcal Software). A P value <0.05 was considered significant.

RESULTS

Effects of DAM and Cyto D on APD_{90}. DAM and Cyto D had differential effects on transmembrane APD_{90}. Figure 1 shows an example of DAM causing a concentration-dependent shortening of APD_{90}, which was reversible upon washout. In contrast, Cyto D did not significantly affect APD_{90} at concentrations that varied from 10 to 40 μmol/l. Table 1 shows the results of all RV studied. With concentrations of 5, 10, 15, and 20 mmol/l, DAM reduced APD_{90} by 37.7%, 38.3%, 45%, and 48.3%, respectively ($P < 0.001$ for all comparisons). The effects were reversible upon washout. In contrast, Cyto D had no significant effect on the APD_{90} at any of concentrations studied (Table 1).

Effects of DAM and Cyto D on slopes of APDR curves. At baseline, the mean maximal slopes of the APDR curves without DAM and Cyto D were 1.14 ± 0.38 and 1.29 ± 0.45, respectively (P = not significant, NS). With increasing concentrations, DAM progressively decreased the maximum slope of APDR, whereas Cyto D showed no such effect (Fig. 2). DAM reduced the maximal slopes of APDR curves in a concentration-dependent manner (Table 1). In contrast, there was no significant change in the slope of APDR curves in any of concentrations of Cyto D studied (Table 1).

Effects of DAM and Cyto D on spatiotemporal complexity of VF. Figure 3 summarizes the effects of DAM and Cyto D on the spatiotemporal complexity of VF. According to our previous studies (12, 19), Poincaré plots have four patterns corresponding to four different degrees of complexity in VF: formless, cloudlike appearance (highest in complexity, black); signet, ringlike appearance (higher complexity, crosshatch); cluster (lower complexity, parallel lines); and point (lowest complexity, white) (Fig. 3*C*). The Poincaré plots had either a formless, cloudlike appearance or signet ringlike appearance at baseline. With increasing concentrations of DAM (Fig. 3*A*), there was a progression from a higher complexity to lower complexity. At 20 mmol/l of DAM, the VF always converted to VT and Poincaré plots showed point patterns (lowest complexity). This pattern was reversible upon washout. On the other hand, a higher complexity persisted for all concentrations of Cyto D (Fig. 3*B*). Figure 3, *D* and *E*, shows typical pseudoelectrocardiograms and TMP recordings with their associated Poincaré plots shown in Fig. 3*C*. During baseline VF, pseudoelectrocardiograms and TMP recordings show highly variable amplitudes and interactivation intervals. These patterns were converted to periodic rhythm with higher concentrations of DAM.

Kolmogorov entropy. The results of our KE calculations are shown in Table 1 by the two methods (17, 19). In both methods, entropy decreased significantly with increasing DAM and then sharply increased at washout. We also applied two statistical tests. First, we dropped the last (equals washout) point from each data set and tested the remaining six points for correlation. In every data set, by both methods, there was a statistically significant ($P < 0.001$) negative correlation with sequence position. In other words, the KE decreased significantly with increasing DAM. Second, to test the significance of the washout, for each of the two methods of calculation of KE, we considered the six KE values for the washout point and compared them with the six average values for the prewashout data by using Student's *t*-tests. In both methods, the prewashout KE values were significantly higher than the washout KE values. There were also excellent correlations between the maximum slope of the APDR curve and the KE *method A* ($r = 0.93$, $P = 0.007$) and KE *method B* ($r = 0.98$, $P = 0.001$). Whereas, in the Cyto D group, KE values did not show statistically significant changes from baseline to increasing Cyto D concentrations to a 60-min period of superfusion with Cyto D-free Tyrode solution (Table).

Effects of DAM and Cyto D on number of wavelets. All RV in VF at baseline had multiple wavelets within the mapped region (3.4 ± 0.6 in DAM group and 3.4 ± 0.5 in Cyto D group). With increasing concentrations of

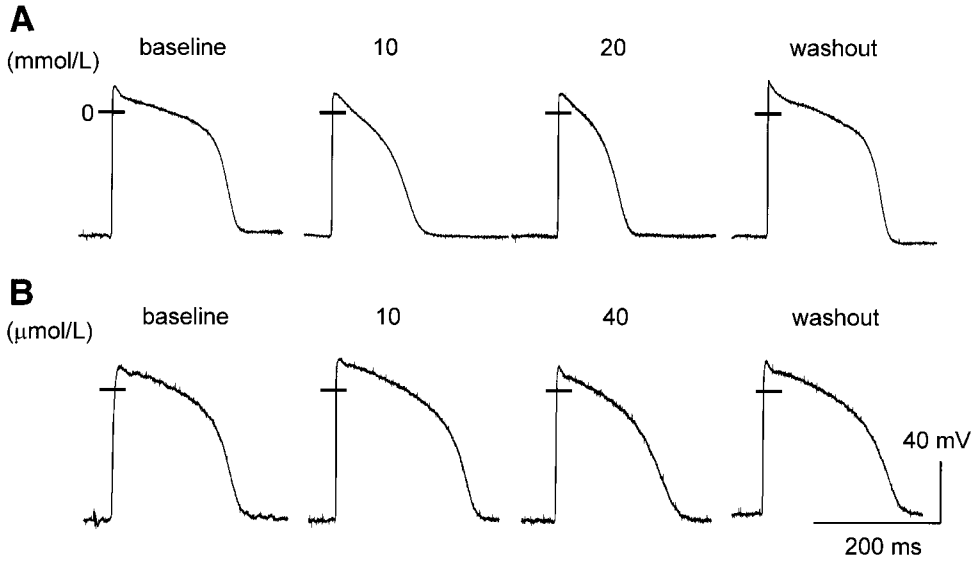

Fig. 1. Transmembrane potentials recorded from the epicardium of swine right ventricles (RV). Diacetyl monoxime (DAM) causes concentration-dependent, reversible action potential duration measured to 90% repoloarization (APD_{90}) shortening (*A*). Cytochalasin D (Cyto D) has little effect on the APD_{90} (*B*).

Table 1. *Effects of DAM and Cyto D on dynamics of VF*

	Effects of DAM, mmol/l					
	Control	5	10	15	20	Washout
APD_{90} at 400 ms CL, ms	197.2 ± 27.4	122.8 ± 18.8*	121.7 ± 20.6*	108.5 ± 17.4*	102.0 ± 16.2*	174.9 ± 16.4
dV/dt_{max} at 400 ms CL, V/s	63.2 ± 41.7	84.6 ± 52.2	96.2 ± 14.0	82.7 ± 33.4	72.4 ± 41.0	121.1 ± 41.8
Resting membrane potential at 400 ms CL, mV	−64.4 ± 14.1	−68.8 ± 10.5	−70.5 ± 5.5	−69.5 ± 12.2	−60.2 ± 11.7	−74.3 ± 9.3
AP amplitude at 400 ms CL, mV	74.4 ± 10.0	77.3 ± 17.3	74.1 ± 7.0	72.6 ± 10.4	65.7 ± 11.3	82.3 ± 7.8
Shortest DI during dynamic APDR curve determination, ms	31.9 ± 14.8	49.1 ± 21.4	48.5 ± 10.2	49.7 ± 15.7	64.7 ± 17.1†	28.8 ± 10.1
Max slope of APDR curve	1.14 ± 0.38	0.71 ± 0.25*	0.50 ± 0.22*	0.33 ± 0.24*	0.21 ± 0.14*	0.77 ± 0.22
Kolmogorov entropy (*model A*)	8.72 ± 0.49	8.36 ± 1.13*	6.71 ± 1.36*	5.75 ± 1.18*	4.94 ± 0.30*	8.34 ± 0.32
Kolmogorov entropy (*model B*)	0.34 ± 0.15	0.22 ± 0.20*	0.07 ± 0.09*	0.06 ± 0.08*	0.01 ± 0.01*	0.25 ± 0.16
Dominant frequency, Hz	11.2 ± 1.8	9.1 ± 3.3	9.3 ± 3.7	9.2 ± 2.3	9.6 ± 1.9	9.6 ± 0.8
No. of wavelets	3.4 ± 0.6	2.7 ± 0.8*	1.8 ± 0.8*	1.4 ± 0.7*	1.0 ± 0.0*	2.8 ± 0.8

	Effects of Cyto D, μmol/l				
	Control	10	20	40	Washout
APD_{90} at 400 ms CL, ms	189.8 ± 27.4	175.6 ± 30.6	189.2 ± 34.2	184.2 ± 36.0	196.2 ± 44.0
dV/dt_{max} at 400 ms CL, V/s	63.9 ± 38.7	87.9 ± 46.1	76.5 ± 38.9	71.6 ± 11.4	85.8 ± 35.2
Resting membrane potential at 400 ms CL, mV	−66.1 ± 9.0	−64.1 ± 13.5	−65.4 ± 12.0	−72.6 ± 7.3	−76.7 ± 13.4
AP amplitude at 400 ms CL, mV	72.6 ± 12.8	76.4 ± 14.7	75.2 ± 13.8	76.44 ± 6.1	77.2 ± 20.8
Shortest DI during dynamic APDR curve determination, ms	41.2 ± 8.8	38.6 ± 10.8	44.2 ± 15.3	52.5 ± 37.6	49.3 ± 38.9
Max slope of APDR curve	1.29 ± 0.45	1.29 ± 0.61	1.34 ± 0.54	1.10 ± 0.54	1.47 ± 0.84
Kolmogorov entropy (*model A*)	7.73 ± 0.35	7.83 ± 0.32	7.69 ± 0.45	7.30 ± 0.56	7.48 ± 0.34
Kolmogorov entropy (*model B*)	0.32 ± 0.13	0.30 ± 0.12	0.41 ± 0.22	0.31 ± 0.18	0.29 ± 0.19
Dominant frequency, Hz	11.0 ± 2.7	9.9 ± 1.8	9.3 ± 2.3	9.0 ± 2.7	8.6 ± 1.6
No. of wavelets	3.4 ± 0.5	3.2 ± 0.6	3.2 ± 0.6	3.2 ± 0.6	3.2 ± 0.5

Values are means ± SD. APD_{90}, action potential duration at 90% repolarization; CL, cycle length; dV/dt_{max}, maximal voltage change over time; DI, diastolic interval; APDR, APD restitution. Max, indicates maximum. *$P < 0.001$ compared with control; †$P < 0.01$ compared with control.

DAM, the mean number of wavelets progressively decreased (Table 1). In contrast, Cyto D had no such effect (Table 1). Figure 4*A* shows the number of wavelets at baseline, after 20 mmol/l of DAM perfusion, and after washout in a typical experiment. Figure 4, *B* and *C,* shows corresponding fluorescent signals and TMP recordings, respectively. With 20 mmol/l of DAM, the optical map usually showed a repetitive monomorphic planar wave front propagating from outside of the optical field to the other side of the field except in one episode, which showed a stationary spiral wave (Fig. 5) that persisted for >30 s.

DISCUSSION

In this study, we found that DAM results in concentration-dependent reduction of APD_{90} and of the slope of APDR curves in isolated swine RV. These changes are associated with progressively reduced numbers of VF wave fronts and lesser dynamic complexity of VF as measured by KE. At high concentrations, DAM converts VF to VT. In contrast, Cyto D has no effect on APDR curves or the dynamics of VF. These results are compatible with the restitution hypothesis of VF and suggest that DAM may be unsuitable as an E-C uncoupler for optical mapping studies of VF.

Restitution hypothesis of VF. The restitution hypothesis (36) states that APDR is a critical factor in the generation and maintenance of VF and that targeting cardiac restitution could lead to effective antifibrillatory intervention. The argument that a steeply sloped APDR curve creates instabilities during rapid pacing was first made by Nolasco and Dahlen (27). Subsequently, many investigators demonstrated that APDR is important in the generation of alternans, which lead to the development of ventricular arrhythmias, including VF [see a recent review by Weiss et al. (36)]. A quantitative measure of APDR is through the construction of an APDR curve and the calculation of the maximum slope of that curve. A slope ≥1 is needed to create the dynamic instability that promotes the generation of wavebreak and VF. As a result, chemical agents that flatten the APDR curve (such as verapamil, DAM, or bretylium) decrease VF complexity (6, 30), prevent the induction of VF, and convert existing VF into a periodic rhythm (13, 30).

DAM and Cyto D. DAM is a commonly used chemical agent to induce E-C uncoupling during optical mapping studies (1, 9, 10, 14, 20, 28). Liu et al. (26) previously reported that DAM (5–20 mmol/l) decreased APD_{90} and the refractory period in a concentration-dependent manner. Riccio et al. (30) expanded these observations and showed the DAM may convert VT to VF at concentrations commonly used for optical mapping studies. Both DAM and Cyto D reduce contraction. Biermann et al. (3) found that, in isolated canine right ventricular trabeculae, DAM at 10 mmol/l and

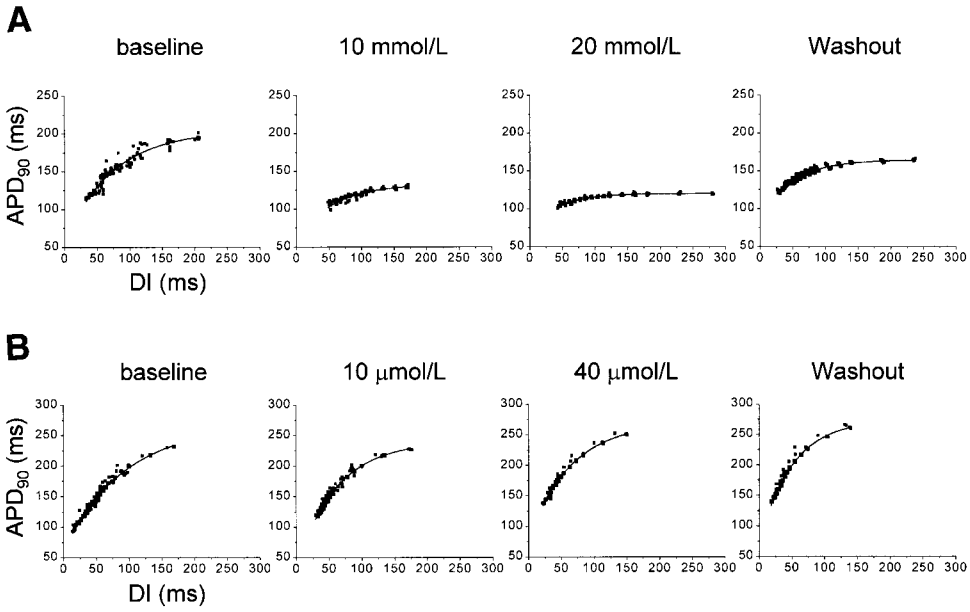

Fig. 2. Effects of increasing concentrations of DAM (*A*) and Cyto D (*B*) on the dynamic APD restitution curves determined from a swine RV epicardium. DI, diastolic interval.

Cyto D at 80 μmol/l were equally effective in reducing peak isometric force to 10 ± 3% and 8 ± 1%, respectively. Wu et al. (38) studied different concentrations of Cyto D on contraction in a canine left ventricular wedge preparation. The concentration used in that study was 10, 15, 20, 25, 30, 35, and 40 μmol/l. They showed that all the concentration of Cyto D could reduce arterial pulses to 1/*e* of its initial value. The authors suggested that Cyto D concentration between 20 and 30 μmol/l in the perfusate represented the range of the most usage-efficient dose for effective immobilization of ventricular muscle. Our study showed that, whereas both Cyto D (10–40 μmol/l) and DAM (5–20 mmol/l) reduce contraction, only DAM has significant effects on APDR curve and APD.

The mechanisms of the action of DAM are complex. DAM has been found to reduce L-type Ca^{2+} current in rabbit (26), rat (8), and guinea pig (16) ventricular myocytes and to decrease delayed rectifier K^+ current in rabbit (26) and rat myocytes (8), leading to net shortening of APD and refractory periods in cats (37), sheep (26), guinea pigs (16, 26), and dogs (2, 3) but action potential lengthening in rats (7). In comparison, Cyto D, an F-actin disrupter, has no significant effect

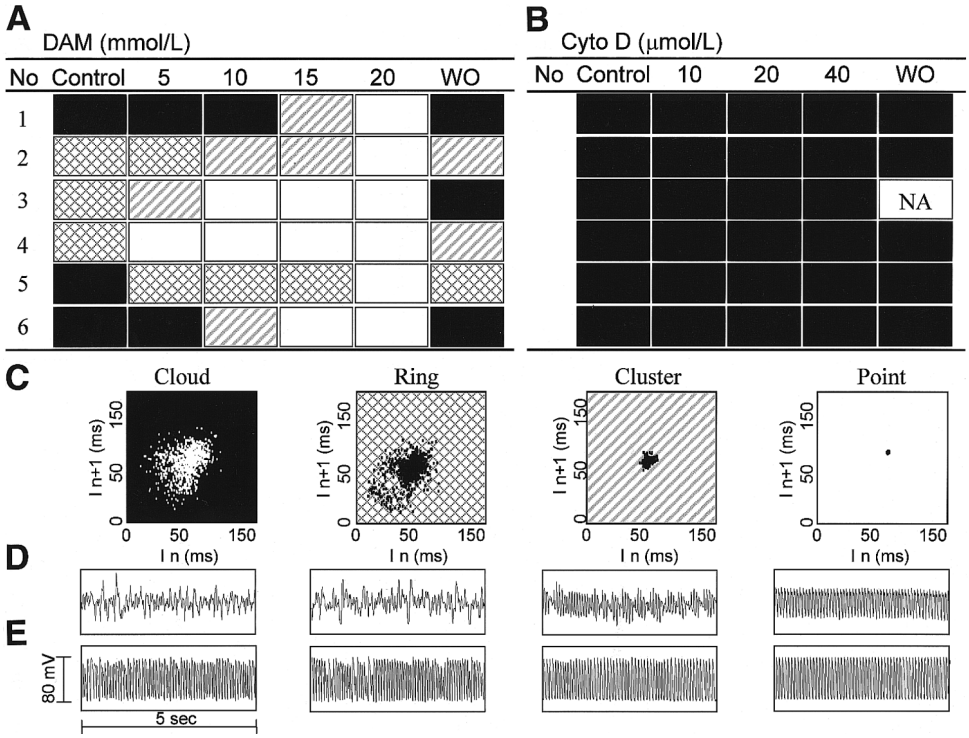

Fig. 3. Effects of DAM (*A*) and Cyto D (*B*) on spatiotemporal complexities of ventricular fibrillation (VF). *C*: Poincaré plots of 4 patterns corresponding to 4 different degrees of complexity in VF. *D* and *E*: typical pseudoelectrocardiogram and transmembrane potential (TMP) recordings, respectively. See text for details.

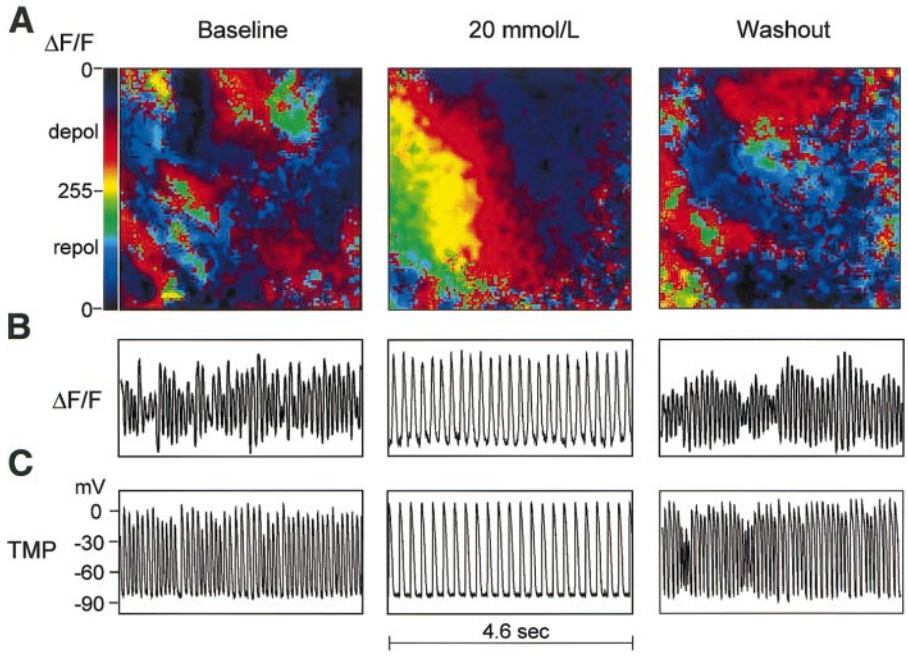

Fig. 4. Effects of DAM on wavelet number and TMP recordings. *A*: snap shots of membrane potential determined by optical mapping. We used color spectrum to represent membrane potentials. Black colors represent repolarized tissue just before the upstroke of the action potential. The color turns red as the membrane is depolarized. When the action potential reaches its peak, the color turns yellow. The color then gradually changes from yellow to green, then blue, and eventually back to black during repolarization. The wavelets were considered to be different if they had different directions of propagation and were separated from each other by blue or black areas. At 20 mmol/l of DAM, monomorphic tachycardia was induced in all preparations. There were multiple wavelets during VF at baseline (wavelet number = 4) and after washout (wavelet number = 3). However, with 20 mmol/l of DAM, there was a single large wave front that repetitively invade the mapped region from left lower corner of the mapped tissue. *B* and *C*: corresponding fluorescent signals and single cell TMPs, respectively, of the activation maps shown in *A*. depol, Depolarization; repol, repolarization.

on action potential parameters in dogs (3) but lengthens APD and hyperpolarizes the cardiac membrane in mouse myocytes (18). In our study, DAM reversibly shortened APD_{90} and depressed the slope of APDR curve, similar to the experiment of Riccio et al. (30). We also found that DAM decreased the degree of spatiotemporal complexity and increased periodicity in a concentration-dependent manner. At high concentrations it converted VF to VT. All those effects were reversible 30 min after washout with DAM-free Tyrode solution. In contrast, Cyto D had no significant effect on the slope of the APDR curve and did not change either the patterns of activation or the KE. From these results, we suggest that Cyto D may be used as an E-C uncoupler for optical mapping studies of VF. DAM should be avoided in those studies.

Alternative mechanisms for VF to VT transition. In addition to the restitution hypothesis, two other hypotheses have been proposed to explain the mechanisms of VF. One is the wavelength hypothesis (29), which states that the length of excitation wave (the product of refractory period and conduction velocity) is an important determinant for reentry. Lengthening of the wavelength is antiarrhythmic, while shortening

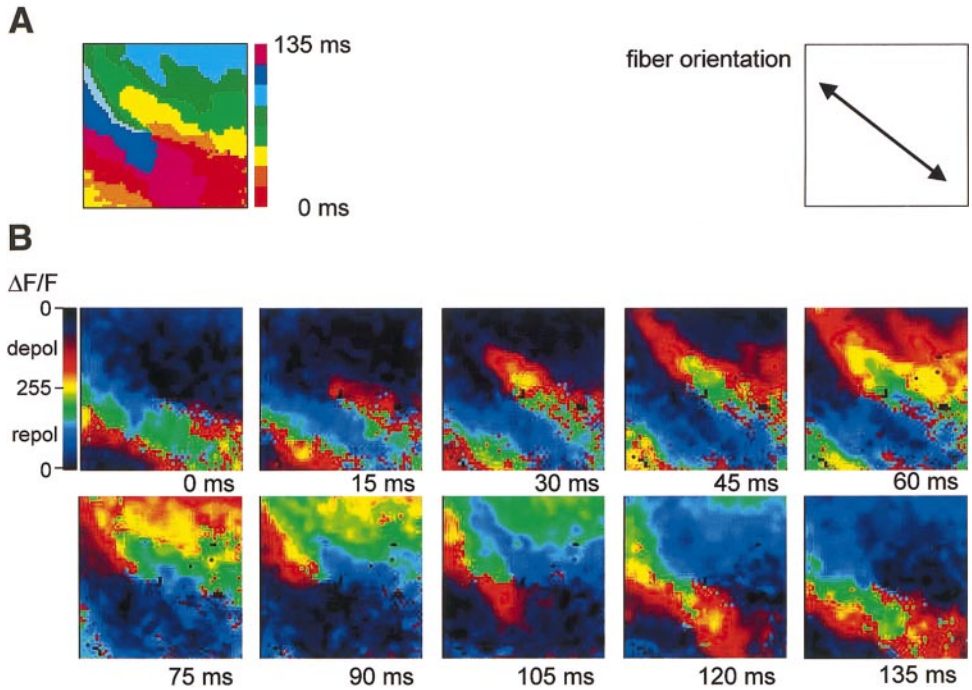

Fig. 5. Stationary spiral wave induced after 20 mmol/l of DAM perfusion. *A*: isochrone map of the activation sequences shown in *B* (time = 0 to 135 ms). Red is the first activated site and purple is the last.

the wavelength is proarrhythmic. However, in the present study we found that DAM shortens APD but converts VF to VT. Samie et al. (32) showed that verapamil, a calcium channel blocker that shortens APD, is also effective in converting VF to VT. One possible explanation of these findings is that calcium is a major contributor to TMP at sites of slow propagation (22), for example, near the core of reentry when the wave front curvature is steep. Because of this action, calcium channel blockade enlarges the core of reentry, lengthens the cycle length, and converts VF to VT (32). This mechanism could explain the effects of DAM on VF observed in the present study.

Implications on VF mapping. The present study also has significant implications on optical mapping of VF. Chen and colleagues (5) reported that reentrant wave fronts in VF are short-lived, lasting on average only a few rotations before they terminate spontaneously or by wave-wave interaction (4). Similarly, reentrant wave fronts during Wiggers' stage II VF are also short-lived, with an average life span of 3.2 rotations in canine ventricles (23). Rogers et al. (31) later reported even an shorter life span (1.5 rotations) for the reentrant wave fronts on the epicardium of the swine ventricles. Because of its very short life span and uncommon occurrence, Rogers et al. (31) suggested that sustained reentry is transmural or that mechanisms governing sustained reentry are relatively unimportant to the dynamics of VF.

Using optical mapping studies in the presence of DAM, Gray et al. (14, 15) studied VF in rabbit ventricles and reported that the reentrant wave fronts (spiral waves) might be sustained for a much longer period of time than that reported by Rogers et al. (31). A single sustained meandering spiral wave may result in variations of activation CL at various parts of the ventricles through the Doppler effect (14, 15). The electrocardiogram at that time is indistinguishable from VF. The authors conclude that a single rapidly meandering spiral wave may cause cardiac fibrillation. A discrepancy between the VF activation patterns mapped with electrode mapping techniques and with optical mapping techniques therefore exists. The use of DAM in optical mapping studies may partially explain some of this difference.

Limitations of the study. Whereas Cyto D does not alter APD or flatten the APDR curve, it does reduce peak sodium currents in ventricular myocytes (34), which may in turn reduce conduction velocity and decrease the wavelength. Although Wu et al. (38) previously reported that Cyto D at a steady concentration of 10 μmol/l did not alter transmural conduction velocity, it is unclear whether conduction velocity is reduced when a higher concentration of Cyto D is used. It would be interesting to study the effects of Cyto D on conduction velocity at the concentrations used in this study. However, Frasier et al. (11) studied transmural activation patterns during epicardial and endocardial pacing. They found that activation in both cases is primarily endocardial to epicardial because of rapid endocardial conduction. These data indicate that the impulse propagation from one point to another on the epicardium may be much longer than the distance between these two points. Because optical mapping techniques cannot be used to study three-dimensional transmural propagation of activation, we were not able to accurately determine the conduction velocity. This is a limitation of the study.

A second limitation was that two different optical mapping systems were used in the study. The system used for mapping Cyto D had slightly better spatial and temporal resolution than that used for mapping VF during DAM infusion. However, both mapping systems have sufficient resolution to determine the number of wave fronts present in the tissue. Furthermore, the effects of DAM and Cyto D on the dynamics of VF were also evaluated with entropy, pseudoelectrocardiograms, and TMP recordings. All showed consistent findings. Therefore, we do not think a difference of mapping system resolution invalidated the conclusions of the study.

We thank Avile McCullen, Nina Wang, and Meiling Yuan for technical assistance and Elaine Lebowitz for secretarial assistance.

This study was done during the tenure of a Fellowship Grant from the College of Medicine, Yonsei University, Seoul, Korea (to M.-H. Lee), a grant from the Myung Sun Kim Memorial Foundation (to M.-H. Lee), a Cedars-Sinai ECHO Foundation Award (to H. S. Karagueuzian), the Kawata and the Laubisch Endowments (to J. N. Weiss), and a Pauline and Harold Price Endowment (to P.-S. Chen). This study also was supported in part by National Heart, Lung, and Blood Institute Grants P50-HL-52319, R01-HL-58533, R01-HL-66389; American Heart Association National Center Grant-in-Aid 9750623N and 9950464N, a UC-TRDRP 9RT-0041; and the Ralph M. Parsons Foundation (Los Angeles, CA).

REFERENCES

1. **Banville I, Gray RA, Ideker RE, and Smith WM.** Shock-induced figure-of-eight reentry in the isolated rabbit heart. *Circ Res* 85: 742–752, 1999.
2. **Bergey JL, Reiser J, Wiggins JR, and Freeman AR.** Oximes: "enzymatic" slow channel antagonists in canine cardiac Purkinje fibers? *Eur J Pharmacol* 71: 307–319, 1981.
3. **Biermann M, Rubart M, Moreno A, Wu J, Josiah-Durant A, and Zipes DP.** Differential effects of cytochalasin D and 2,3-butanedione monoxime on isometric twitch force and transmembrane action potential in isolated ventricular muscle: implications for optical measurements of cardiac repolarization. *J Cardiovasc Electrophysiol* 9: 1348–1357, 1998.
4. **Cha YM, Birgersdotter-Green U, Wolf PL, Peters BB, and Chen PS.** The mechanisms of termination of reentrant activity in ventricular fibrillation. *Circ Res* 74: 495–506, 1994.
5. **Chen PS, Wolf PD, Dixon EG, Danieley ND, Frazier DW, Smith WM, and Ideker RE.** Mechanism of ventricular vulnerability to single premature stimuli in open-chest dogs. *Circ Res* 62: 1191–1209, 1988.
6. **Chorro FJ, Canoves J, Guerrero J, Mainar L, Sanchis J, Such L, and Lopez-Merino V.** Alteration of ventricular fibrillation by flecainide, verapamil, and sotalol: an experimental study. *Circulation* 101: 1606–1615, 2000.
7. **Coulombe A, Lefevre IA, Deroubaix E, and Coraboeuf E.** Effect of diacetyl monoxime on transient outward current in rat ventricular myocytes. *Pflügers Arch* 414: S173–S174, 1989.
8. **Coulombe A, Lefevre IA, Deroubaix E, Thuringer D, and Coraboeuf E.** Effect of 2,3-butanedione 2-monoxime on slow inward and transient outward currents in rat ventricular myocytes. *J Mol Cell Cardiol* 22: 921–932, 1990.
9. **Davidenko JM, Pertsov AM, Salomonsz R, Baxter W, and Jalife J.** Stationary and drifting spiral waves of excitation in isolated cardiac tissue. *Nature* 355: 349–351, 1992.

10. **Efimov IR, Cheng Y, Van Wagoner DR, Mazgalev T, and Tchou PJ.** Virtual electrode-induced phase singularity: a basic mechanism of defibrillation failure. *Circ Res* 82: 918–925, 1998.
11. **Frazier DW, Krassowska W, Chen PS, Wolf PD, Danieley ND, Smith WM, and Ideker RE.** Transmural activations and potentials on three-dimensional anisotropic canine myocardium. *Circ Res* 63: 135–146, 1988.
12. **Garfinkel A, Chen PS, Walter DO, Karagueuzian HS, Kogan B, Evans SJ, Karpoukhin M, Hwang C, Uchida T, Gotoh M, Nwasokwa O, Sager P, and Weiss JN.** Quasiperiodicity and chaos in cardiac fibrillation. *J Clin Invest* 99: 305–314, 1997.
13. **Garfinkel A, Kim YH, Voroshilovsky O, Qu Z, Kil JR, Lee MH, Karagueuzian HS, Weiss JN, and Chen PS.** Preventing ventricular fibrillation by flattening cardiac restitution. *Proc Natl Acad Sci USA* 97: 6061–6066, 2000.
14. **Gray RA, Jalife J, Panfilov A, Baxter WT, Cabo C, Davidenko JM, and Pertsov AM.** Nonstationary vortexlike reentrant activity as mechanism of polymorphic ventricular tachycardia in the isolated rabbit heart. *Circulation* 91: 2454–2469, 1995.
15. **Gray RA, Jalife J, Panfilov AV, Baxter WT, Cabo C, Davidenko JM, Pertsov AM, and Hogeweg P.** Mechanisms of cardiac fibrillation. *Science* 270: 1222–1223, 1995.
16. **Gwathmey JK, Hajjar RJ, and Solaro RJ.** Contractile deactivation and uncoupling of crossbridges. Effects of 2,3-butanedione monoxime on mammalian myocardium. *Circ Res* 69: 1280–1292, 1991.
17. **Hilborn RC.** *Chaos and Nonlinear Dynamics*. 1994, p. 386–390.
18. **Jalife J, Morley GE, Tallini NY, and Vaidya D.** A fungal metabolite that eliminates motion artifacts. *J Cardiovasc Electrophysiol* 9: 1358–1362, 1998.
19. **Kim YH, Garfinkel A, Ikeda T, Wu TJ, Athill CA, Weiss JN, Karagueuzian HS, and Chen PS.** Spatiotemporal complexity of ventricular fibrillation revealed by tissue mass reduction in isolated swine right ventricle. Further evidence for the quasiperiodic route to chaos hypothesis. *J Clin Invest* 100: 2486–2500, 1997.
20. **Knisley SB, Hill BC, and Ideker RE.** Virtual electrode effects in myocardial fibers. *Biophys J* 66: 719–728, 1994.
21. **Kolmogorov AN.** A new metric invariant of transitive dynamical systems and automorphisms in Lebesgue spaces. *Dokl Acad Nauk SSSR* 119: 861–864, 1958.
22. **Laurita KR, Singal A, and Rosenbaum DS.** High-resolution optical mapping of intracellular calcium and transmembrane potential during reentry (Abstract). *Pacing Clin Electrophysiol* 22: 702, 1999.
23. **Lee JJ, Kamjoo K, Hough D, Hwang C, Fan W, Fishbein MC, Bonometti C, Ikeda T, Karagueuzian HS, and Chen PS.** Reentrant wave fronts in Wiggers' stage II ventricular fibrillation: characteristics, and mechanisms of termination and spontaneous regeneration. *Circ Res* 78: 660–675, 1996.
24. **Lin SF, Roth BJ, and Wikswo JP Jr.** Quatrefoil reentry in myocardium: an optical imaging study of the induction mechanism. *J Cardiovasc Electrophysiol* 10: 574–586, 1999.
25. **Lin SF and Wikswo JP Jr.** Panoramic optical imaging of electrical propagation in isolated heart. *J Biomedical Optics* 4: 200–207, 1999.
26. **Liu Y, Cabo C, Salomonsz R, Delmar M, Davidenko J, and Jalife J.** Effects of diacetyl monoxime on the electrical properties of sheep and guinea pig ventricular muscle. *Cardiovasc Res* 27: 1991–1997, 1993.
27. **Nolasco JB and Dahlen RW.** A graphic method for the study of alternation in cardiac action potentials. *J Appl Physiol* 25: 191–196, 1968.
28. **Pertsov AM, Davidenko JM, Salomonsz R, Baxter WT, and Jalife J.** Spiral waves of excitation underlie reentrant activity in isolated cardiac muscle. *Circ Res* 72: 631–650, 1993.
29. **Rensma PL, Allessie MA, Lammers WJEP, Bonke FIM, and Schalij MJ.** Length of excitation wave and susceptibility to reentrant atrial arrhythmias in normal conscious dogs. *Circ Res* 62: 395–410, 1988.
30. **Riccio ML, Koller ML, and Gilmour RFJ.** Electrical restitution and spatiotemporal organization during ventricular fibrillation. *Circ Res* 84: 955–963, 1999.
31. **Rogers JM, Huang J, Smith WM, and Ideker RE.** Incidence, evolution, and spatial distribution of functional reentry during ventricular fibrillation in pigs. *Circ Res* 84: 945–954, 1999.
32. **Samie FH, Mandapati R, Gray RA, Watanabe Y, Zuur C, Beaumont J, and Jalife J.** A mechanism of transition from ventricular fibrillation to tachycardia: effect of calcium channel blockade on the dynamics of rotating waves. *Circ Res* 86: 684–691, 2000.
33. **Sinai YG.** On the concept of entropy of a dynamical system. *Dokl Acad Nauk SSSR* 124: 768–778, 1959.
34. **Undrovinas AI, Shander GS, and Makielski JC.** Cytoskeleton modulates gating of voltage-dependent sodium channel in heart. *Am J Physiol Heart Circ Physiol* 269: H203–H214, 1995.
35. **Voroshilovsky O, Qu Z, Lee MH, Ohara T, Fishbein GA, Huang HL, Swerdlow CD, Lin SF, Garfinkel A, Weiss JN, Karagueuzian HS, and Chen PS.** Mechanisms of ventricular fibrillation induction by 60-Hz alternating current in isolated swine right ventricle. *Circulation* 102: 1569–1574, 2000.
36. **Weiss JN, Garfinkel A, Karagueuzian HS, Qu Z, and Chen PS.** Chaos and the transition to ventricular fibrillation: a new approach to antiarrhythmic drug evaluation. *Circulation* 99: 2819–2826, 1999.
37. **Wiggins JR, Reiser J, Fitzpatrick DF, and Bergey JL.** Inotropic actions of diacetyl monoxime in cat ventricular muscle. *J Pharmacol Exp Ther* 212: 217–224, 1980.
38. **Wu J, Biermann M, Rubart M, and Zipes DP.** Cytochalasin D as excitation-contraction uncoupler for optically mapping action potentials in wedges of ventricular myocardium. *J Cardiovasc Electrophysiol* 9: 1336–1347, 1998.